PERFORMANCE INVESTIGATION ON SCAN-ON-RECEIVE AND ADAPTIVE DIGITAL BEAM-FORMING FOR HIGH-RESOLUTION WIDE-SWATH SYNTHETIC APERTURE RADAR

F. Bordoni, M. Younis, E. Makhoul Varona, N. Gebert, G. Krieger

Microwaves and Radar Institute (IHR), German Aerospace Center (DLR), Oberpfaffenhofen, Germany;
E-mail: federica.bordoni@dlr.de; Tel: +49 (0)8153 28 3301; Fax: +49 (0)8153 28 1449

ABSTRACT

Intensive research is currently ongoing in the field of Smart Multi-Aperture Radar Technique (SMART) for Synthetic Aperture Radar (SAR). This work investigates the performance of the SMART SAR system for high-resolution wide-swath imaging based on Scan-on-Receive (SCORE) algorithm for receive beam steering. SCORE algorithm works under model mismatch conditions in presence of topographic height. A study on the potentiality of an adaptive approach for receive beam steering based on spatial spectral estimation is presented. The impact of topographic height on SCORE performance in different operational scenarios is examined, with reference to a realistic SAR system. The SCORE performance is compared to that of the adaptive approach by using the Cramèr Rao lower bound analysis.

1. INTRODUCTION

Spaceborne SAR for remote sensing applications is experiencing a golden age, as testified by the number of the recent and forthcoming missions, e.g. ALOS PALSAR, TerraSAR-X, COSMO-SkyMed, RADARSAT-2, TanDEM-X, Sentinel-1. Nevertheless, the current generation of spaceborne SAR sensors suffers a basic limitation: it does not allow for high resolution imaging and, simultaneously, wide coverage and high radiometric resolution [1]. For instance, a spatial resolution around 1 m could be achieved over a swath width of 10 km; whereas coverage of 200 km allows for SAR final products[1] with a resolution in the order of 100 m [2]. The importance for many remote sensing applications to overcome this limitation has motivated an intensive research within the frame of SMART (see [3, 4] and the references therein).

Main characteristics of SMART SAR systems are the employment of Smart antennas [5], i.e. the use of multiple transmit/receive channels and the introduction of digital signal processing techniques, such Digital Beam-Forming (DBF), in the conventional SAR processing [3, 4, 6]. In fact, Smart antennas allow a relaxation of SAR system design constraints by

increasing the degrees of freedom, which results in lower ambiguity level, higher signal-to-noise ratio (SNR) and improved radiometric resolution, and a mitigation of the trade-off between swath width and spatial resolution [3, 4, 6]. It is worth noting that the intrinsic huge quantity of information associated with high-resolution and wide-swath imaging, together with redundancies involved by the multichannel acquisition, could place critical requirements on the downlink data rate.

Among SMART SAR, the system proposed by Suess *et al.* [7, 8], denoted as HRWS, merges the advantages of an extensive illumination capability with the high gain and directivity of a large antenna, and combines the flexibility offered by a multi-channel architecture with a limited download data volume. The HRWS SAR system is based on an algorithm for steering of the elevation beam pattern, called SCORE: a wide swath is illuminated by using a small transmit antenna; whereas in reception a large multi-channel antenna and DBF are employed in order to obtain a sharp and high gain pattern, which follows the pulse echo as it travels along the ground swath. The steering direction of the receive pattern corresponds to the expected direction of arrival (DOA) of the echo, which is assumed *a priori* known. In particular, according to [8], it is computed based on the vertical slant-range plane acquisition geometry, under the hypothesis of a stringent spherical Earth model, i.e. no topographic height is taken into account. Nevertheless, in real acquisition scenarios, characterized by mountains and relief, there will be a displacement between the actual DOA and the steering (i.e. maximum gain) direction; which results in a gain loss with respect to the ideal operational conditions (see Figure 1). Moreover, SCORE steering approach neglects not only the effect of the actual topographic profile along the slant-range elevation plane, but also the effect of surface variations along the azimuth direction.

These observations suggest the option of an Adaptive Digital Beam-Forming (ADBF), i.e. to compute adaptively the steering direction of the receive beam, by (digitally) processing the signals available from the vertical sub-apertures of the multi-channel receive antenna. In fact, the vertical sampling provides a "spatial history" of the signal, which could be used to evaluate the distribution of the received energy as a function of the DOA; then the receive beam steering direction could be selected as the one associated with the strongest

---

[1] The spatial resolution of a final product is further degraded by the multilook processing, mainly necessary to obtain satisfactory radiometric resolution.

signal, eventually within a roughly expected spatial sector.

According to the ADBF approach, the receive beam steering algorithm is cast into the frame of *spatial spectral estimation* and *DOA estimation*. This topic has been extensively studied in array signal processing theory [9, 10], and also with reference to the Interferometric SAR application [11]. Nevertheless, the HRWS SAR spaceborne application shows specific challenges. First, the processing of the signals available from the vertical sub-apertures should be performed onboard, in order to reduce the downlink data volume. This requires to dealing with wideband signals and imposes additional constraints on the complexity of the processing method [10, 12]. Moreover, in case of wide illuminated swaths, the useful signal could be superimposed to range-ambiguous echoes having a power comparable with that of the signal of interest. Finally, instrument parameters, such as dimension of the antenna, number of elements, noise level (NESZ), whose values strongly affect the ultimate estimation performance, do not allow for many degrees of freedom, due to imaging requirements and physical/economical constraints.

This paper shows the effect of topographic height on conventional, not adaptive, SCORE performance: the steering displacement and the corresponding gain loss introduced by topography are analyzed as a function of the acquisition geometry and of the receive antenna architecture and pattern shape, with reference to a realistic SAR system operational scenario. Moreover, in order to evaluate the potentiality of an ADBF for spaceborne high-resolution wide-swath SAR systems, a performance analysis based on Cramér Rao Lower Bound (CRLB) is developed [9, 10]. The performance of SCORE and ADBF are compared vs. the main SAR system parameters.
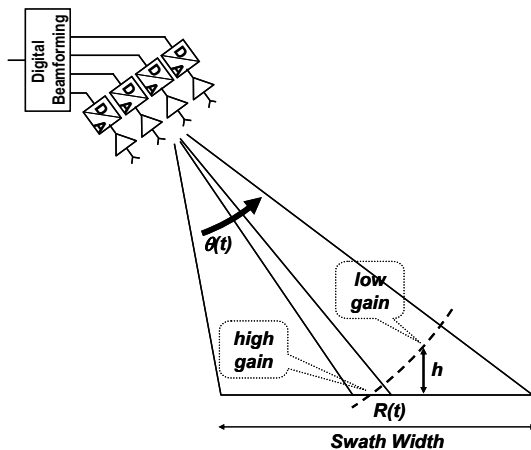

Fig. 1. SCORE in presence of topographic height.

2. REVIEW OF SCAN-ON-RECEIVE

The HRWS SAR system employs a small transmit antenna and a large receive antenna, which is split in multiple sub-apertures, arranged according to a uniform linear array (ULA) geometry in azimuth and elevation [7, 8]. The small transmit aperture is used to illuminate a large swath; the large receiving antenna allows for ambiguity suppression and compensation for the reduced transmit antenna gain. In particular, the conflict between swath width and azimuth resolution is overcome by using M sub-apertures located along the azimuth direction, according to the displaced phase center antenna (DPCA) technique; whereas the SAR radiometric resolution is improved by using multiple sub-apertures in elevation, and by processing the corresponding signals by SCORE algorithm. In detail, according to [8], the echo DOA is computed based on the vertical slant-range plane acquisition geometry, assuming a stringent spherical Earth model (no topographic elevation). Under this assumption, in fact, the DOA of the echo received from a point-like target is univocally associated to the two-way time delay, τ [8]:

$$\vartheta(\tau) = \mathrm{acos}\left\{ \frac{4\left(H_{orb} + R_E\right)^2 - 4R_E^2 + \left(c_0\tau\right)^2}{4\left(H_{orb} + R_E\right)c_0\,\tau} \right\} \qquad (1)$$

where, ϑ denotes the DOA measured w.r.t. the nadir angle, H_{orb} is the orbit height; R_E the Earth radius; c_0 the light speed. Then a time-varying DBF is used to combine the signals received by the elevation sub-apertures, in order to obtain, at each instant, a sharp and high gain beam, steered towards the expected DOA of the backscattering echo[2]. The DBF reduces the data rate by eliminating the redundancies; the high gain SCORE beam results in an increased SNR, compensating the low gain (wide beam) of the transmit antenna. Specifically at the swath edges (half-power beamwidth angles) the typical two-way loss of a conventional system is reduced.

3. BEHAVIOUR OF SCORE IN PRESENCE OF TOPOGRAPHIC HEIGHT

In presence of topographic height, h, SCORE works under model mismatch conditions: there is an *angular displacement*, $\Delta\vartheta$, between the actual DOA of the received echo, ϑ_{act}, and the SCORE steering direction, ϑ_s, computed according to eq. (1):

$$\Delta\vartheta = \vartheta_{act} - \vartheta_s(\tau_{act}), \qquad (2)$$

---

[2] In case of long chirp pulses an additional frequency dependent beam steering is included in SCORE [8, 9]. In the rest of the paper, we assume that SCORE frequency dependent beam steering allows recovering all the pulse energy with the maximum gain, when the DOA of the pulse centre is correctly recovered [8, 9].

where, τ_{act} denotes the actual two-way time delay of the received echo. This results in a loss of performance. In fact, the echo impinging on the receive antenna is not weighted by the maximum of the receive beam, as expected in ideal (no topographic height) conditions. The degradation of SCORE performance due to topographic height is here quantified by the parameter *Pattern Loss (PL)*, defined as the value of the normalized receive beam pattern, which weights the echo backscattered from a source located at a topographic height, h :

$$PL = \frac{C^R(\vartheta_s + \Delta\vartheta)}{C^R(\vartheta_s)} \qquad (3)$$

where, $C^R(\vartheta)$ indicates the value of the elevation receive beam pattern generated by DBF corresponding to the angle ϑ .

In order to evaluate the effect of surface elevation on a realistic HRWS SAR system, the reference HRWS SAR system described in Table 1 has been considered. This system allows for a spatial resolution and swath width in the order of 1 m and 70 km, respectively, a NESZ below – 22 dB, range ambiguity (RASR) below – 30 dB and azimuth ambiguity (AASR) below -26 dB.

Figures 2 and 4 show the angular displacement and the PL as a function of the ground-range position (of the projection on the Earth surface) of the backscattering source, parameterized vs. the source topographic height, h . Values of h between 0 m and 8000 m have been considered.

As shown in Figure 2, the angular displacement depends on the acquisition geometry. The main effect is related to the surface height: for the reference system, the angular displacement varies between 0.15° for h=1000 m and 1.45° for h=8000 m. For a fixed height, the displacement weakly decrease for increasing ground range positions. The extent of the PL depends on the receive beam shape.

PARAMETER	UNIT	VALUE
Geometry		
Orbit Height	km	520
Antenna Tilt Angle, β	deg	32.25
Swath Limits	deg	[29.6, 34.9]
(look ang., ground range)	km	[300, 370]
Radar Parameters		
PRF	Hz	1775
RF Center Frequency	GHz	9,65
Pulse Bandwidth	MHz	250
Av. Tx Power	W	1100
TX Antenna		
Height	m	0.50
Length	m	2.45
RX Antenna		
Height	m	1.5
Nr. of sub-apert. in el.		15 (x 0.10 m)
Length	m	9.8
Nr. of sub-apert. in az.		7

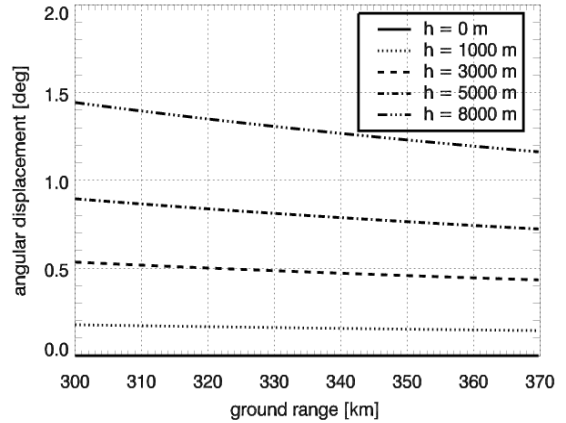**Tab. 1.** Reference HRWS SAR system parameters.

Fig. 2. SCORE angular displacement, in presence of topographic height, h.
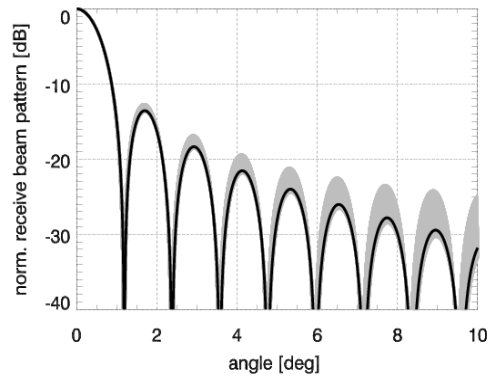

Fig. 3. Elevation receive beam patterns generated by DBF during the scansion of the swath vs. the elevation angle (instantaneous steering direction reported to the origin).
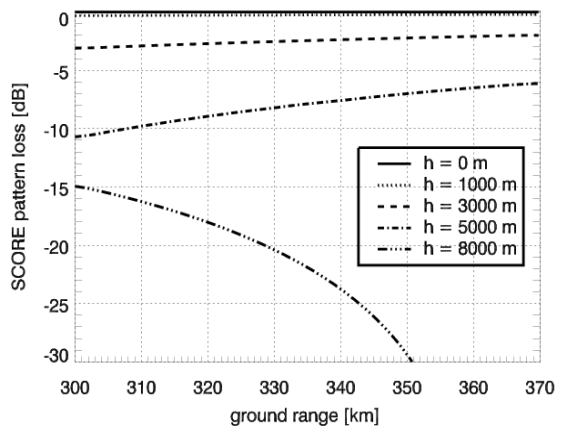

Fig. 4. SCORE pattern loss in presence of topographic height, h.

In particular, for the reference HRWS SAR, the half power beam width (HPBW) of the receive beam is in the order of 1° (see Figure 3). SCORE PL, obtained as the value of the normalized receive pattern corresponding to

the steering displacement, is plotted in Figure 4. The PL curves show that loss is moderate for topographic height below 1000 m; nevertheless a loss of several dB could be reached when no information about topographic height is used to steer the beam.

4. ADAPTIVE DIGITAL BEAM-FORMING

According to SCORE, the received pattern is steered towards the DOA of the received signal, assumed *a priori* known. Nevertheless, a critical loss of performance could occur when no information about the actual backscattering geometry is conveyed in the steering mechanism. An alternative approach is to steer the receive beam towards an estimate of the actual DOA, obtained by processing the signal echo impinging on the multiple sub-apertures, arranged according to a ULA geometry along the elevation direction.

As explained in the introduction, the wideband nature of the SAR pulses and the constraints on the algorithm complexity do not allow a direct application of simple spectral estimation methods, such as Beamforming or Capon, which have been successfully applied in radar array processing [9, 10] and also in multichannel Interferometric SAR (InSAR) [11]. On the other hand, the methods conceived for broadband signal are computationally demanding for onboard processing [10, 12].

In the following, a pre-processing procedure, which allows to trace the SAR signal back to a signal model typically used in narrowband spectral estimation [9, 10], is proposed. For simplicity, the explanation refers initially to a point-like target and is afterward generalized.

Assume that the transmitted SAR pulse is a chirp:

$$s(t) = rect\left(\frac{t}{T}\right)\cos\left[2\pi\left(f_c t + \frac{\kappa}{2}t^2\right)\right], \quad (4)$$

where T is the chirp duration, κ the chirp rate, f_c the RF center frequency. The two-way time delay of the echo, received by the $k-th$ sub-aperture in elevation from a point-like target located in the vertical slant-range plane, could be written as:

$$\tau_k = \tau_0 + \frac{d \cdot k \cdot \sin(\beta - \vartheta)}{c_0}, \qquad k = 0, \cdots, K-1, \quad (5)$$

where τ_0 denotes the two-way time delay of the pulse at the first $(k=0)$ receive sup-aperture, d is the distance between the phase centers of two adjacent sub-apertures, K the number of elevation sub-apertures of the receive antenna, ϑ is the echo DOA and β the antenna tilt angle, both measured respect to the nadir. Then, the equivalent baseband signal of the echo at the $k-th$ sub-aperture could be written as:

$$r_k(t) = \alpha \cdot rect\left(\frac{t-\tau_k}{T}\right)\exp\left\{j\pi\kappa(t-\tau_k)^2\right\}\exp\left\{-j2\pi f_c\tau_k\right\},$$

$$k = 0, \cdots, K-1 \quad (6)$$

where, α is the complex amplitude accounting for the propagation and backscattering mechanism. Note that from here on t indicates a discrete time variable.

After range compression with a matched filter to the transmit chirp and the application of a coregistration processing [13], the signal in (6) could be written as:

$$r_k(t) = \alpha \cdot \text{sinc}\left\{\kappa \cdot T \cdot (t-\tau_0)\right\} \cdot \exp\left\{-j \cdot 2\pi f_c\tau_k\right\}, \quad (7)$$

where, for simplicity, we use the same symbols as in (6) for the signal and the complex constant. Then considering the time-sample corresponding to the time delay, $t = \tau_0$:

$$r_k = \alpha \cdot \exp\left\{-j2\pi\frac{d}{\lambda}\sin(\beta-\vartheta)k\right\}, k = 0, \cdots, K-1 \quad (8)$$

where λ denotes the radar wavelength, and without loss of generality, the factor $\exp\left\{-j2\pi f_c\tau_0\right\}$ has been included in the complex constant α.

Eq. (8) could be rewritten by using a vector notation and taking into account the additive thermal noise, which corrupts the useful signal:

$$\mathbf{y} = \alpha \cdot \mathbf{a}(\vartheta) + \mathbf{v}, \quad (9)$$

where, $\mathbf{y}$, $\mathbf{a}(\vartheta)$, and $\mathbf{v}$ are K-dimensional complex vectors, and the element $k-th$ is associated to the $k-th$ sub-aperture. In particular, $\mathbf{v}$ collects the thermal noise contribute, $\mathbf{a}(\vartheta)$, whose $k-th$ element is given by

$$[\mathbf{a}(\vartheta)]_k = \exp\left\{-j2\pi\frac{d}{\lambda}\sin(\beta-\vartheta)k\right\}, \quad (10)$$

denotes the steering vector of the pulse impinging on the array, which collects the information of the DOA.

It is worth comparing the echo received at the same sub-aperture from different, subsequent pulse transmissions: the echo DOA changes in a negligible way for $N < 100$ multiple consecutive azimuth acquisitions[3]; moreover, the effect of range cell migration on the time delay, i.e. on the position of the recorded samples corresponding to the same backscattering source, could be easily computed and compensated onboard. These observations allow considering different equivalent *snapshots* or *looks*, n, of the signal in eq. (9):

$$\mathbf{y}(n) = \alpha \cdot \mathbf{a}(\vartheta) + \mathbf{v}(n), \ n = 1, \cdots, N. \quad (11)$$

Eq. (11) could be generalized by introducing multiple, N_s, backscattering sources:

$$\mathbf{y}(n) = \sum_{i=1}^{N_s} \alpha_i \cdot \mathbf{a}(\vartheta_i) + \mathbf{v}(n), \ n = 1, \cdots, N. \quad (12)$$

---

[3] For the typical satellite parameters system, the maximum DOA variation due to the azimuth platform displacement is in the order of 10^{-5} deg.

117

In fact, in general, multiple echoes of the transmitted SAR pulses impinge on the receive antenna simultaneously, due to preceding or succeeding pulses with time-delays separated by a multiple of the PRF or backscattering sources in layover. When extended homogeneous backscattering sources are considered, the signal component in eq. (12) could be written as [11, 14]:

$$\alpha_i \cdot \mathbf{a}(\vartheta_i) = \sqrt{\tau_i} \mathbf{a}(\vartheta_i) \otimes \mathbf{x}_i(n), \ n = 1, \cdots, N, \quad (13)$$

where, $\otimes$ denotes the Hadamard product; τ_i denotes the texture, i.e. the mean power level of each source, and $\mathbf{x}_i$ the speckle [11].

The problem of evaluating the distribution of the received energy as a function of the DOA is now traced back to the narrowband spectral estimation, and can be expressed as the estimation of the spatial power spectral density (PSD) of the data in eq. (12).

In order to statistically describe the signal in eq. (12-13), it is useful to recall to the model used in multichannel InSAR for the pixel complex amplitude, $\mathbf{y}(n)$, collected by the K sensors array [11, 14]:

$$\mathbf{y}(n) = \sum_{i=1}^{N_S} \sqrt{\tau_i} \mathbf{a}(\varphi_i) \otimes \mathbf{x}_i(n) + \mathbf{v}(n), \ n = 1, \cdots, N \quad (14)$$

where, N the number of independent looks; $\mathbf{v}$ the thermal noise contribute, modeled as a complex Gaussian spatially white process, with zero mean and power σ_v^2; N_s denotes the number of extended homogeneous backscattering sources in layover; $\mathbf{a}(\varphi)$ the spatial steering vector; φ_i the source interferometric phase[4] (directly related to the DOA), modeled as an unknown constant; τ_i, is the radar reflectivity or texture, modeled as a real, positive, unknown deterministic parameter; $\mathbf{x}_i$ the speckle, modeled as complex correlated Gaussian random vector with a zero mean, unit variance and covariance matrix $\mathbf{C}_i$; with $\mathbf{x}_i(n_p)$ independent of $\mathbf{x}_i(n_q)$ when $n_p \neq n_q$, for $i = 1, \cdots, N_s$.

In the following analysis we will refer to the statistical model of eq. (14). This means that we consider an illuminated swath characterized, along the iso-range lines, by a homogeneous backscattering surface and constant topographic height. Though simple, this reference surface allows for a first comparison between SCORE and ADBF achievable performance.

5. BEHAVIOUR OF ADBF: CRAMÉR RAO LOWER BOUND

The achievable performance of the ADBF could be evaluated by CRLB analysis, based on the model in eq.

---

[4] The interferometric phase is defined as the phase difference between the furthest phase centers of the array [11].

(14). In fact, the value of the CRLB on the estimate of the DOA provides the minimum variance of any unbiased estimator of ϑ_i [9, 10]. Then, in analogy with the SCORE angular displacement in eq. (2), it could be defined an angular displacement between the actual DOA of the echo and that estimated by ADBF as:

$$\Delta\vartheta = \sqrt{CRLB\{\hat{\vartheta}_i\}}, \quad (15)$$

where $\sqrt{CRLB\{\hat{\vartheta}_i\}}$ denotes the square root of the CRLB on the estimate of ϑ_i, i.e. the standard deviation of the estimated DOA, $\hat{\vartheta}_i$. The pattern loss can be computed according to eq. (3) for the angular displacement in eq. (15).

For the CRLB computation and performance analysis, it is assumed that the speckle covariance matrix is:

$$\begin{aligned}
\left[\mathbf{C}_i\right]_{u,v} &= E\left\{\left[\mathbf{x}_i(n)\right]_u \cdot \left[\mathbf{x}_i(n)\right]_v^H\right\} \\
&= \begin{cases} 1 - \dfrac{|u-v|}{K-1} \cdot H_i & \text{for } |u-v| \leq \dfrac{(K-1)}{H_i} \\ 0 & \text{otherwise} \end{cases}
\end{aligned} \quad (16)$$

where $E\{\}$ denotes the mean statistical value, $(\cdot)^H$ the conjugate transpose operator, $H_i = H_{ant}/H_{ci}$ the normalized antenna's height, given by the ratio between the size of the receive antenna along the elevation direction, H_{ant}, and the critical antenna height, H_{ci}, for which the $i-th$ source decorrelates at the extremities of the array [11, 14, 15].

The CRLB on the DOAs, $\{\vartheta_i\}_{i=1}^{N_s}$, can be derived as in [11], particularizing the data model (14) for the DOA, ϑ_i, through the relationship with the interferometric phase, φ_i as:

$$\varphi_i = -4\pi \frac{d(K-1)}{\lambda} \sin(\beta - \vartheta_i), \quad (17)$$

and considering the speckle covariance matrix, $\mathbf{C}_i$, as defined in (16).

6. PERFORMANCE COMPARISON

This section shows a comparison between the performance achievable with SCORE and ADBF. The performance is evaluated in terms of angular displacement and pattern loss. The reference HRWS SAR described in Table 1 is considered. Moreover, a reference acquisition scenario is assumed, which is characterized by the following parameters: two extended homogeneous backscattering sources, $N_s = 2$, located respectively at 304.42 km and 317.87 km ground range

(30.0° and 31.05° off-nadir angle[5]), with a topographic height of 3000 m; both sources have the same mean power, such that the corresponding signal-to-noise ratio at the output of the array, $SNR_i = K \tau_i / \sigma_v^2$, is equal to 9 dB; the normalized antenna height, H_i, is in the order of 1.8e-4 for both sources[6]; the number of consecutive azimuth acquisitions, or *independent looks*, is $N = 5$ (this value allows to completely neglect the range cell migration effect). Starting from this reference acquisition scenario/system, the performance of SCORE and ADBF are evaluated as a function of single parameters of interest, by keeping constant the other parameters value. The results corresponding to the reference scenario are indicated by an asterisk in each figure.

Figures 5 show the performance as a function of the topographic height. For the ADBF the angular displacement is about 0.11°, with a trend *almost* non sensitive to the topographic variation; the corresponding pattern loss is negligible. SCORE angular displacement increases proportionally to the height value, till 1.4° for a topographic height of 8000 m. SCORE pattern loss increases till a value of -25 dB for a height of 7000 m. It must be noted that for 7000 m the PL is higher than for 8000 m, because the displacement for the case of 7000 m approaches the first null of the receive pattern, whereas in the case of 8000 m the signal is acquired with the first secondary lobe (see Figure 3). It is worth noting that the performance of ADBF is negligibly affected by the location of the sources along the swath. Figure 6 reports the angular displacement as a function of the SNR of the first source (# 1), $SNR_1 = K \tau_1 / \sigma_v^2$. For ADBF, the accuracy on the estimation of ϑ_1 improves as a function of the SNR_1; whereas for SCORE it remains unaltered.

The SNR threshold, where the performance of the ADBF becomes better w.r.t. the conventional SCORE is around 0 dB. Figure 7 investigates the effect of source angular separation. As expected, SCORE performance is constant. The performance of ADBF is better than that of SCORE, for a source separation greater than about half of the HPBW. Figures 8 investigate the impact of the height of the receive antenna. The number of sub-apertures is constant, $K = 15$, i.e. the antenna size variation implies also a variation of the sub-aperture spacing (inter-element spacing). The angular displacement of ADBF degrades as the antenna becomes shorter. In fact, the reduced separation between the sub-apertures induces a low sensitivity (all the sub-apertures "observe" approximately the same signal). The antenna height $H_{ant} = 1m$ corresponds to the lower limit, where the performance of ADBF is better than that of SCORE. The angular displacement of SCORE is constant, nevertheless the corresponding PL degrades as the

antenna height increases due to the reduced mainlobe width of the receive beam. Figure 9 shows the performance as a function of the number of sub-apertures in elevation, while the antenna size in elevation is constant, $H_{ant} = 1.5\,\text{m}$. The availability of multiple sub-apertures does not affect the accuracy of ADBF estimation, at least when the sources are sufficiently distant (see Figure 7). For instance, when the DOA separation is about 0.5 HPBW, the use of $K = 4$ in spite than 15 sub-apertures degrades the angular displacement from 0.45° to 0.69°. It is worth noting that a low number of sub-apertures reduces the angular unambiguous range (with $H_{ant} = 1.5\,m$ it is about 17° for $K = 15$, and 5° for $K = 4$). As a consequence, possible echos of preceding or succeeding pulses could fold over the source of interest, reducing the estimation performance. Figure 10 investigates the effect of decorrelation, showing the performance as a function of the normalized antenna height. The performance of ADBF degrades for increasing normalized antenna height: for values greater than 0.8 the ADBF performance is worse than that of SCORE. The previous results are obtained by considering the reference value of number of looks, $N = 5$, which allows neglecting any effect of range cell migration and avoiding the corresponding onboard processing. It is worth noting that the square root of the CRLB, i.e. ADBF angular displacement, reduces for increasing number of looks as the square root of N [9, 10]. Figure 11 shows the angular displacement as a function of the number of looks: for the reference system parameters, the use of a higher number of looks it is not justified. Nevertheless, the use of a higher number of looks could be useful in critical acquisition conditions, such as low SNR and high decorrelation.

7. CONCLUSIONS

The impact of topographic height on SCORE performance has been examined with reference to a realistic SAR system. The numerical results show that the loss is moderate for topographic height below 1000 m; nevertheless a loss of several dB could occur when no information about the topographic height is used to steer the receive beam. An adaptive approach, ADBF, for receive beam steering based on spatial spectral estimation has been proposed. The achievable performance of ADBF have been investigated by the Cramèr Rao lower bound analysis and compared to those of SCORE versus the main system parameters. The numerical analysis shows that ADBF outperforms SCORE and reaches promising results in most of the analyzed scenarios.

---

[5] The angular separation between the DOAs of the two sources corresponds to the HPBW of the receive beam.

[6] The critical height, H_{ci}, is in the order of 8.3 km, assuming no local slope [15].

8. REFERENCES

[1] J. C. Curlander, R. N. McDonough, "Synthetic Aperture Radar: Systems and Signal Processing", NY, Wiley, 1991.

[2] S. Mezzasoma, A. Gallon, F. Impagnatiello, G. Angino, S. Fagioli, A. Capuzi, F. Caltagirone, R. Leonardi, U. Ziliotto, "COSMO-SkyMed system commissioning: End-to-end system performance verification", *Proc. IEEE Radar Conference, RADAR '08*, pp. 1092-1096, May 2008.

[3] G. Krieger, N. Gebert, A. Moreira, "Multidimensional Waveform Encoding: A New Digital Beamforming Technique for Synthetic Aperture Radar Remote Sensing", *IEEE Trans. on Geosci. and Remote Sens.*, vol. 46, no. 1, pp.31-46, Jan. 2008.

[4] M. Younis, F. Bordoni, N. Gebert, G. Krieger, "Smart Multi-Aperture Radar Techniques for Spaceborne Remote Sensing", *Proc. IEEE Geosci. and Remote Sens. Symp., IGARSS'08*, July 2008.

[5] M. Chryssomallis, "Smart Antennas", *IEEE Antennas and Propagation Magazine*, Vol. 42, No. 3, pp. 129-136, June 2000.

[6] N. Gebert, G. Krieger, and A. Moreira, "Digital Beamforming on Receive: Techniques and Optimization Strategies for High-Resolution Wide-Swath SAR Imaging", *IEEE Trans. on Aerosp. and Electron. Syst.*, 2008, accept. for publication.

[7] M. Suess, B. Grafmueller, R. Zahn, "A novel high resolution, wide swath SAR system," *Proc. IEEE Int. Geosci. and Remote Sens. Symp.*, IGARSS´01, vol. 3, pp. 1013-1015, July 2001.

[8] M. Suess and W. Wiesbeck, "Side-Looking Synthetic Aperture Radar System", European Patent Application, EP 1 241 487 A1, Sept. 18, 2002.

[9] P. Stoica, R. Moses, "Introduction to Spectral Analysis", Englewood Cliffs, NJ, Prentice-Hall, 1997.

[10] H. L. Van Trees, "Detection, Estimation, and Modulation Theory, Part IV, Optimum Array Processing", John Wiley & Sons, 2002.

[11] F. Gini, F. Lombardini, M. Montanari, "Layover Solution in Multibaseline SAR Interferometry," *Trans. on Aerosp. and Electron. Syst.*, vol. 38, no. 4, pp. 1344-1356, Oct. 2002.

[12] G. Wang, X. -G. Xia, "Iterative Algorithm for Direction of Arrival Estimation with Wideband Chirp Signals", *IEE Proc. Radar, Sonar and Navig.*, vol. 147, no. 5, pp. 233-238, Oct. 2000.

[13] A. Moreira, J. Mittermayer, R. Scheiber, "Extended Chirp Scaling Algorithm for Air- and Spaceborne SAR Data Processing in Stripmap and Scansar Imaging Modes", *Geosci. and Remote Sens.*, vol. 34, no. 5, pp. 1123 – 1136, Sept. 1996.

[14] F. Bordoni, F. Gini, L. Verrazzani, "Capon-LS for Model Order Selection of Multicomponent Interfermetric SAR Signals", *IEE Proceedings Part-F, Radar, Sonar, and Navigation*, vol. 151, no. 5, pp.299 – 305, Oct. 2004.

[15] F. Gatelli, A. M. Guarnieri, F. Parizzi, P. Pasquali, C. Prati, F. Rocca, "The Wavenumber Shift in SAR Interferometry", *IEEE Trans. on Geosc. and Remote Sens.*, vol.32, no. 4, pp. 855 – 865, July 1994.
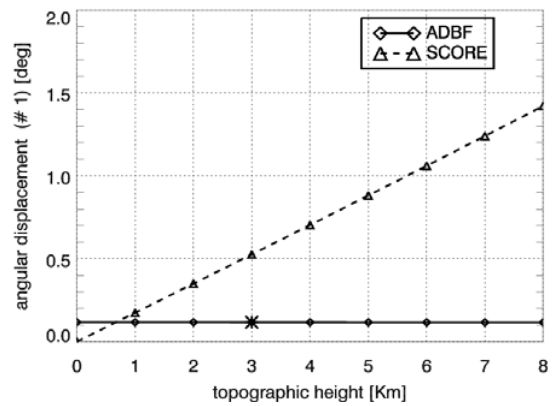
Fig. 5.a. Angular displacement vs. topographic height (const. projection on Earth surface of the source positions).
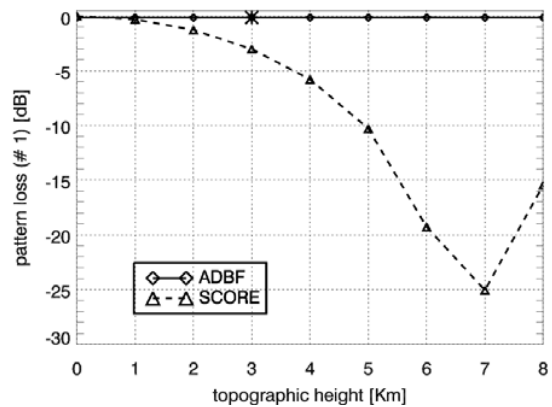

Fig. 5.b. Pattern loss vs. topographic height (const. projection on Earth surface of the source positions).
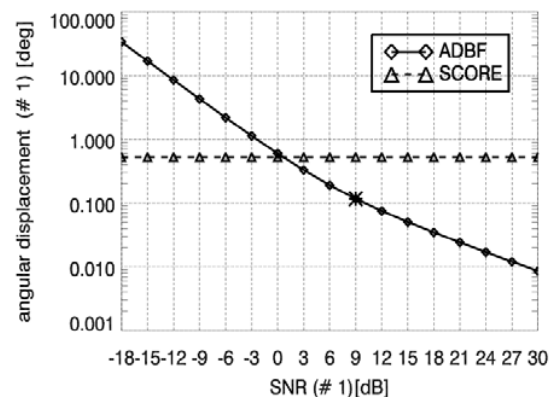

Fig. 6. Angular displacement vs. variation of the SNR of the source #1.
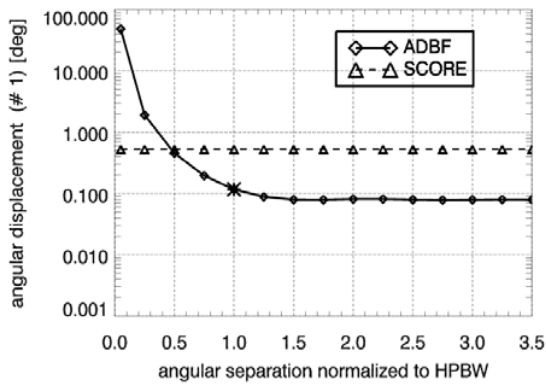
Fig. 7. Angular displacement vs. the angular separation between the two sources normalized to the HPBW (const. position of the source #1).
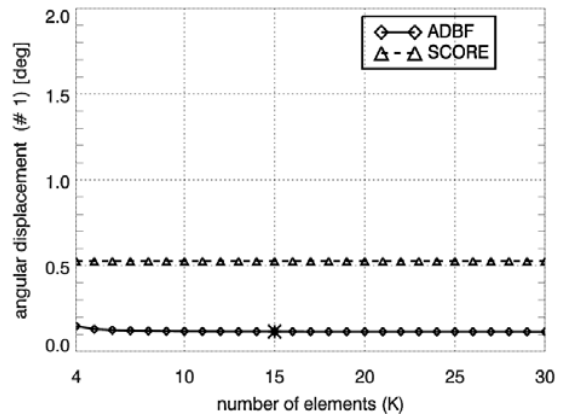

Fig. 9. Angular displacement vs. number of sub-apertures (const. elevation size of the receive antenna).
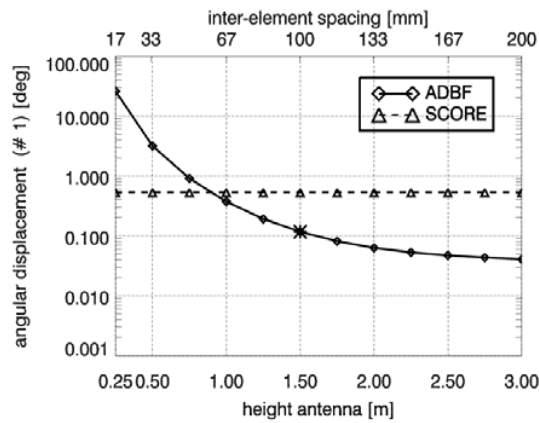

Fig. 8.a. Angular displacement vs. elevation size of the receive antenna (const. number of sub-apertures).
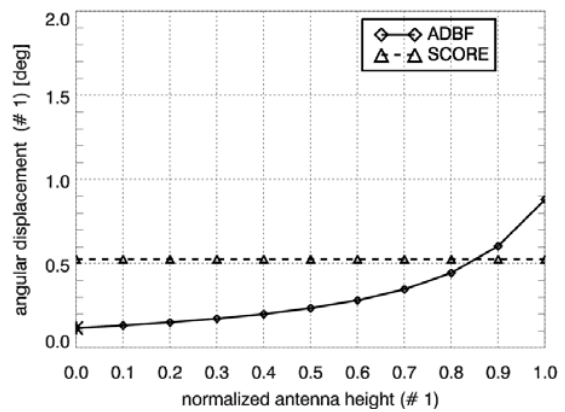

Fig. 10. Angular displacement vs. the normalized antenna height of the source #1.

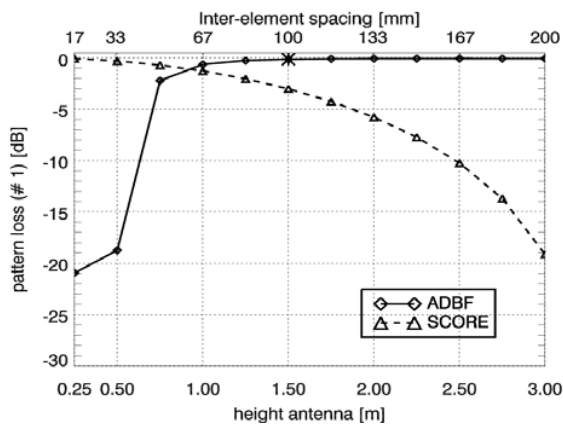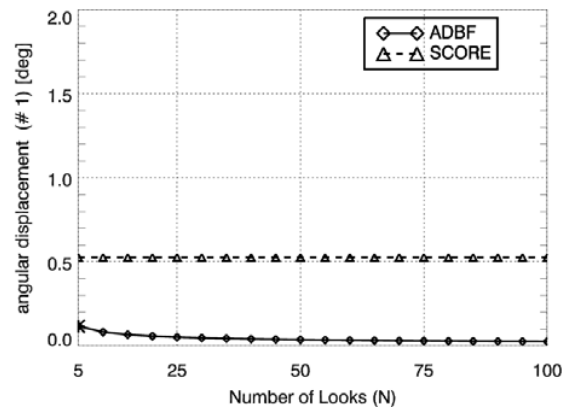**Fig. 8.b.** Pattern loss vs. elevation size of the receive antenna (const. number of sub-apertures).

Fig. 11. Angular displacement vs. number of looks.